# Physical oceanographic conditions during GasEx-2001

Gregory C. Johnson, Christopher L. Sabine, and Kristene E. McTaggart

NOAA Pacific Marine Environmental Laboratory, Seattle, Washington, USA

Julia M. Hummon

Department of Oceanography, University of Hawaii, Honolulu, Hawaii, USA

[1]  GasEx-2001 is a study of air-sea gas exchange in a region of $CO_2$ outgassing. The bulk of the experiment followed a drifting array of near-surface instruments deployed during the second half of February 2001 just south of the equator in the central Pacific Ocean. Physical oceanographic conditions including local currents, the seasonal cycle, Kelvin waves, and tropical instability waves are described using shipboard data and a variety of other data sources to set the large-scale oceanographic context for GasEx-2001. Local physical oceanographic conditions during GasEx-2001 are then analyzed using shipboard data and a simple one-dimensional mixed layer model. The thermocline shoals about 13 m over the 15-day experiment, implying an upwelling rate of $1 \times 10^{-5}$ m s$^{-1}$. Zonal velocity is surface-intensified and westward, with vertical shear mostly through the thermocline. Meridional velocity is also strongly sheared with a maximum equatorward flow in the thermocline that is much reduced by 17-m depth. The mixed layer model exhibits more near-surface warming over the course of the experiment than is observed. Prescribing upwelling in the model closes the heat budget within error estimates. Entrainment at the base of the mixed layer plays a limited role in the mixed layer budgets of carbon and other water properties. Vertical shear of horizontal velocity within the mixed layer and slippage of the array through the surface water also have small (but uncertain) roles in these budgets.     *INDEX TERMS:* 4227 Oceanography: General: Diurnal, seasonal, and annual cycles; 4231 Oceanography: General: Equatorial oceanography; 4504 Oceanography: Physical: Air/sea interactions (0312); 4572 Oceanography: Physical: Upper ocean processes; 4806 Oceanography: Biological and Chemical: Carbon cycling; *KEYWORDS:* equatorial Pacific, upper ocean, mixed layer

**Citation:**  Johnson, G. C., C. L. Sabine, K. E. McTaggart, and J. M. Hummon (2004), Physical oceanographic conditions during GasEx-2001, *J. Geophys. Res.*, *109*, C08S04, doi:10.1029/2002JC001718.

## 1.  Introduction

[2]  GasEx-2001 is a field experiment designed to study air-sea gas exchange in a region of net carbon outgassing. The core of the experiment involved measurements taken by and around a drifting array of near-surface instruments located in recently upwelled water in the central equatorial Pacific Ocean. This portion of the study started at 20:00 UTC 13 February 2001 (yearday 44.85) at 3.00°S, 125.00°W and continued for about 15.5 days until 08:00 UTC 1 March (yearday 60.32). By the end of the study the array had drifted to 2.30°S, 131.54°W, a distance of about 731 km (Figure 1). The NOAA Ship Ronald H. Brown was within a few km of the array throughout much of the experiment. Acoustic Doppler current profiler (ADCP) velocity data and high-quality meteorological data were collected continuously from the ship. The ship occasionally stopped to collect continuous profiles of temperature, salinity, and dissolved oxygen data as a function of pressure with a CTD/$O_2$ (conductivity-temperature-depth,

and oxygen), as well as discrete water samples. From these water samples a variety of biogeochemically relevant water properties were measured. The ship also executed two regional butterfly surveys centered on the array near the start and the middle of the experiment. Each butterfly survey took slightly more than a day to complete. During these surveys the ship ranged as far as 80 km from the array.

[3]  First a wide variety of physical oceanographic phenomena that have potential effects on mixed layer conditions and hence air-sea $CO_2$ flux are described here to set the experiment into a large-scale context, using data collected during the experiment and from other sources. We characterize large-scale oceanographic conditions surrounding GasEx-2001 using a mix of available data including shipboard CTD/ADCP sections, TAO/Triton mooring data, and satellite data. We situate the experiment in terms of the large-scale ocean circulation, seasonal and interannual cycles, tropical instability waves (TIWs) and equatorial Kelvin waves. While only a small fraction of the literature is cited below, a substantial body of work exists on all of these phenomena.

[4]  With the large-scale context set, we then explore the mixed layer evolution in more detail. The budget of carbon
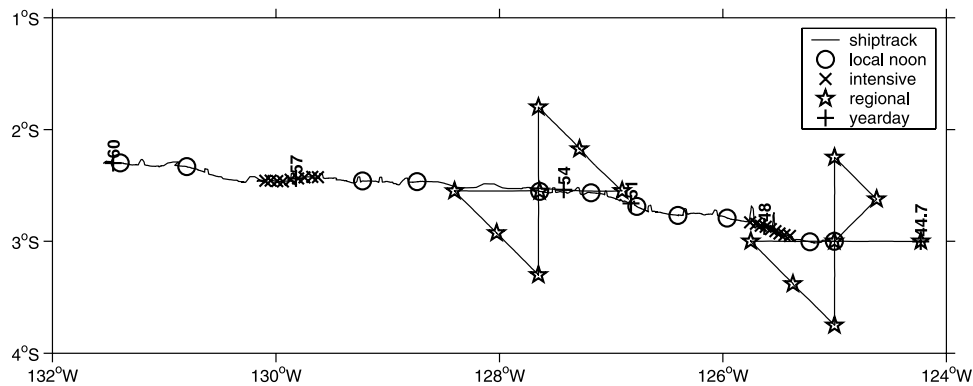
**Figure 1.** Ship track (solid line) and CTD/$O_2$ cast positions during GasEx-2001 including noon casts following the instrument array drift (circles), casts taken following the array during the two intensive observation periods (crosses), and casts taken mostly away from the array during the two regional butterfly surveys (stars). Select times along the track indicated in yeardays (pluses with numbers).

in the mixed layer during the experiment is important for the study of air-sea flux measurements taken during the experiment. Ocean carbon budgets are complex and difficult to close [*Quay*, 1997], and treating all the terms in this budget is beyond this paper, but many of the terms not treated here are analyzed in other papers in this special issue [e.g., *Sabine et al.*, 2004]. The mixed layer carbon budget is of course sensitive to local physical oceanographic conditions, including entrainment at the mixed layer base. Here the CTD/$O_2$ and ADCP data are used to characterize local physical oceanographic conditions during the experiment. Water mass property and velocity distributions, as well as their evolution, are described. Then CTD/$O_2$ profile data (together with dissolved inorganic carbon (DIC) and nutrient data measured from water samples) are used to initialize a simple one-dimensional mixed layer model [*Price et al.*, 1986, hereinafter referred to as PWP].

[5] The PWP model is forced with shipboard meteorological measurements. The evolution of the model mixed layer is compared with observations. The model mixed layer warms slightly more than the observations indicate. Prescribing upwelling at the rate of thermocline shoaling in the model closes the mixed layer heat budget within air-sea flux estimate uncertainties. With this agreement, the effect of mixed layer entrainment on the water properties is assessed. Entrainment of carbon-rich water from below into the mixed layer tends to increase DIC slightly within the mixed layer. The same process affects nutrient and oxygen budgets in the mixed layer. Differential horizontal advection within the mixed layer and slippage of the array through the surface water may also influence the mixed layer carbon, nutrient, and oxygen budgets, and are also discussed below.

## 2. Data

[6] Fifty-one CTD/$O_2$ casts were occupied during GasEx-2001, with 41 taken during the core of the experiment (Figure 1). Data were taken from the surface to 500 dbar and processed to 1-dbar resolution. The CTD/$O_2$ data were calibrated using salinity and oxygen data analyzed from water samples collected with 23 bottles closed on each cast at about 17 nominal pressures, mostly located in the upper 100 dbar. Accuracy of the calibrated CTD/$O_2$ measurements is thought to be about 0.002°C for temperature, 0.003 PSS-78 for salinity, better than 0.1% of full range, or 6 dbar, for pressure (closer to $1-2$ dbar for the shallow casts made during GasEx-2001), and better than 1% of full range, or 2 $\mu$mol kg$^{-1}$, for oxygen. Casts were made near the array at around 20:00 UTC, about local noon, (Figure 1) almost every day except during two regional butterfly surveys when 7 stations were occupied over about a day, many of these far from the array (Figure 1, stars). During two different intensive sampling periods CTD/$O_2$ casts were taken every 3 hours in the vicinity of the array over a 24-hour period (Figure 1, crosses). DIC measurements were made by coulometric titration from water samples, and are thought to be precise to about 2 $\mu$mol kg$^{-1}$. Nutrient measurements made by autoanalyzer from water samples are thought precise to about 1% of full range, or 0.4 $\mu$mol kg$^{-1}$ for nitrate (NO$_3$) and 0.03 $\mu$mol kg$^{-1}$ for phosphate (PO$_4$).

[7] ADCP velocity data were collected throughout the experiment, with one gap in the data lasting about 18 hours in the middle of the experiment. The data were processed in 5 minute by 8-m bins, with the first bin centered at 17 m and good data were collected to a depth of nearly 450 m through much of the experiment. The data are thought to be accurate to at least 0.05 m s$^{-1}$ in both velocity components. Variations in sound speed, as determined by the calibrated CTD/$O_2$ data, were accounted for in the processing. Hourly averages of the data at the full 8-m vertical resolution are used here.

[8] Meteorological data used here to force the one-dimensional mixed layer model include the 10-m wind speed and direction, downwelling shortwave radiation, sea surface albedo, downwelling longwave radiation, upwelling longwave radiation, bulk sensible heat flux, direct latent heat flux, and rain rate. These data are the best available estimates (as of 2 May 2002) of these quantities derived from measurements made using NOAA Environmental Technology Laboratory, Wood Hole Oceanographic Institution, and resident instruments all mounted on the NOAA Ship Ronald H. Brown. The measurements were provided by GasEx-2001 investigators (J. Edson and J. Hare, personal communication, 2002) and are discussed in detail elsewhere in this special issue (W. R. McGillis et al., Air-sea

$CO_2$ exchange in the equatorial Pacific, submitted to *Journal of Geophysical Research*, 2004). The net surface heat flux from these measurements, averaged in 30-min bins, is thought accurate to 10 W m$^{-2}$.

[9] Instrumental accuracies are given for all of these measurements. Spatial and temporal geophysical variability are likely to be much larger, and sampling errors from aliasing this variability are more difficult to quantify.

## 3. Large-Scale Context

[10] Large-scale oceanographic dynamics of the tropical Pacific Ocean have been well understood for some time [*Philander et al.*, 1987]. Easterly trade winds blowing over the region drive westward surface flow on the equator and westward geostrophic flow off the equator (the northern and southern branches of the South Equatorial Current (SEC)) that corresponds to poleward deepening of the thermocline [*Wyrtki*, 1981; *Bryden and Brady*, 1985; *Johnson and McPhaden*, 1999]. As a result, warm water piles up in the west, setting up a thermocline that shoals to the east. The thermocline slope supports a zonal pressure gradient on the equator that drives the Equatorial Undercurrent (EUC) eastward and upward within the thermocline. Off the equator the shoaling thermocline results in equatorward geostrophic flow. The trade winds drive a poleward Ekman transport which overwhelms the geostrophic flow, creating a mean surface divergence near the equator [*Poulain*, 1993; *Johnson*, 2001]. This surface divergence is fed by equatorial upwelling, which is in turn fed in part by zonal convergence of the EUC and in part by meridional geostrophic convergence on the equator [*Weisberg and Qiao*, 2000; *Johnson et al.*, 2001]. The upwelled water is cold, and has a direct feedback on the atmosphere from seasonal to interannual timescales [*Philander*, 1990]. In addition, this upwelled water is also nutrient-rich, oxygen-poor, and carbon-rich, which has a direct impact on biogeochemical [*Feely et al.*, 1999] and biological [*Chavez et al.*, 1999] aspects of climate. Outgassing of these upwelled carbon-rich waters is the focus of GasEx-2001 and this special issue.

[11] Some of the upwelled water flows as far poleward as the subtropics. The cycle of subduction in the subtropics, equatorward geostrophic flow, equatorial upwelling, and poleward surface flow has come to be known as the subtropical cell [*Lu et al.*, 1998]. However, there is also evidence, both from models [*Philander et al.*, 1987] and observations [*Johnson*, 2001; *Johnson et al.*, 2001], that some of the upwelled water is downwelled within $\pm 8°$ latitude of the equator. This downwelling is thought to be confined to the upper thermocline, and the water presumably flows rapidly back to the equator in the geostrophic convergence where it is upwelled again. This shallower, more tropical recirculation has been called the tropical cell. GasEx-2001 is located within the downwelling region of the tropical cell, where recently upwelled, carbon-rich water is present.

### 3.1. Currents and Water Property Distributions

[12] The equatorial system of currents and water property distributions in which GasEx-2001 was situated are revealed by three cross-equatorial CTD/ADCP sections taken within a month of the experiment, in its general vicinity. Prior to the experiment, sections were occupied along 140°W (5°S to 8°N; 19–27 January) and along 125°W (8°S to 8°N; 1–9 February) on the NOAA Ship *Ka'imimoana* during routine maintenance of the TAO/Triton mooring array. A section was also occupied near 135°W (2°S to 5°N; 1–3 March) on the NOAA Ship *Ronald H. Brown* at the conclusion of GasEx-2001, during the steam to Hawaii. In all cases the shipboard ADCP was run continuously, collecting data from about 17 m to over 400 m at 8 m vertical resolution in 5 minute averages, and CTD stations were occupied at least every degree of latitude from the surface to at least 500 dbar at 1 dbar vertical resolution. These data are mapped to a regular latitude depth grid following *Johnson et al.* [2002].

[13] Zonal velocity fields sampled by these sections (Figure 2) reveal the major equatorial currents. Climatologically, in February at these longitudes the EUC is at midstrength and building, the North Equatorial Countercurrent (NECC) is at midstrength and weakening, the north branch of the SEC is at its weakest, and the south branch of the SEC is at its strongest within its limited range of seasonal variation [*Donguy and Meyers*, 1996; *Johnson et al.*, 2002]. In the synoptic sections a robust EUC is centered near the equator and 85–130 m, with maximum zonal velocities of 1.1–1.4 m s$^{-1}$. The SEC is draped over the EUC, with westward flow in the northern branch reaching from 3°–5°N. While the 135°W section does not extend far enough north to sample the NECC, the 125°W and 140°W sections both reveal its eastward flow, found poleward of the northern branch of the SEC. In contrast, meridional velocity fields (Figure 3) do not show the surface Ekman divergence from the equator and the subsurface geostrophic convergence onto the equator that is seen in the mean fields [*Bryden and Brady*, 1985; *Johnson et al.*, 2001] because, as discussed below, vigorous TIW activity overwhelms the weaker mean.

[14] Distributions of potential temperature (Figure 4) and salinity (Figure 5) for these sections reveal that the mixed layer is warmer, fresher, and shallower in the north, under the high precipitation and upwelling favorable wind stress patterns of the Intertropical Convergence Zone [*Delcroix et al.*, 1996]. Salty subsurface water approaches the equator from the south and fresh subsurface water from the north, reflecting the mean geostrophic convergence that feeds the EUC, supplies equatorial upwelling, and maintains a subsurface meridional salinity front along the equator [*Tsuchiya*, 1968; *Johnson and McPhaden*, 1999]. The local subsurface salinity maximum visible in all sections near 1°S is associated with eastward advection of salty water within the EUC contrasting with westward advection of fresher water in the flanking SEC [*Lukas*, 1986]. Along 135°W, where dissolved oxygen was also measured (Figure 6), the highest subsurface dissolved oxygen values on the equator between 100 and 250 m depth are also a signature of eastward water property advection in the EUC [*Tsuchiya*, 1968]. The temperature and salinity fields all show cold and salty chimneys extending up through the mixed layer near the equator (1°N during the 125°W and 135°W sections, and 2°S during the 140°W section). In the 135°W section, the surface waters associated with the chimney at 1°N are also relatively oxygen-poor (only 93% saturated). Surface water does not remain under-
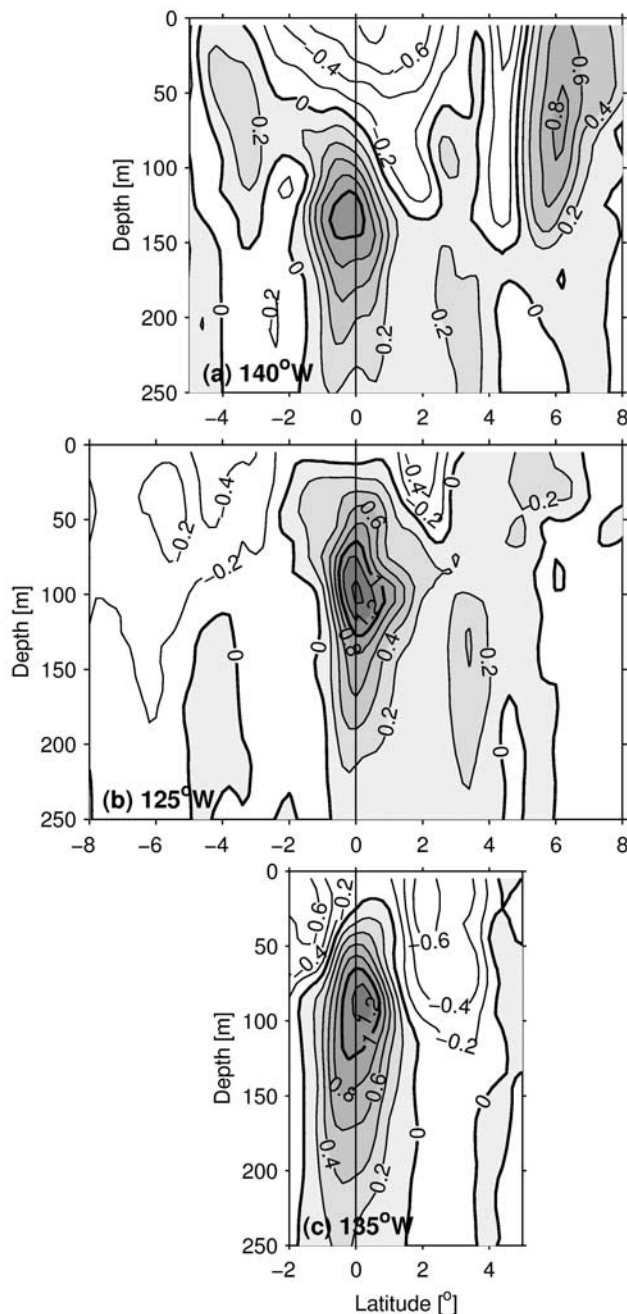
**Figure 2.** Vertical meridional sections of zonal velocity from shipboard ADCP data contoured at 0.2 m s$^{-1}$ intervals against depth [m] and latitude. Increasingly eastward (positive) values are increasingly shaded and isotachs at 1 m s$^{-1}$ intervals are thick. Sections were occupied (a) from 19 to 27 January 2001 nominally along 140°W on the NOAA ship *Ka'imimoana*, (b) from 1 to 9 February 2001 nominally along 125°W on the same ship, and (c) from 1 to 3 March 2001 nominally along 135°W on the NOAA ship *Ronald H. Brown*.

(Figure 3), likely associated with TIWs, were to advect them off the equator.

### 3.2. Interannual and Seasonal Cycles

[15] Mean conditions are unlikely to be representative of synoptic conditions in the ocean due to a number of factors. First, equatorial Pacific conditions vary significantly on interannual timescales, and the phase of the Southern Oscillation Index (SOI) is quite important to conditions in the region, including modulation of $CO_2$ outgassing [*Feely et al.*, 1999]. During GasEx-2001 in February 2001, the
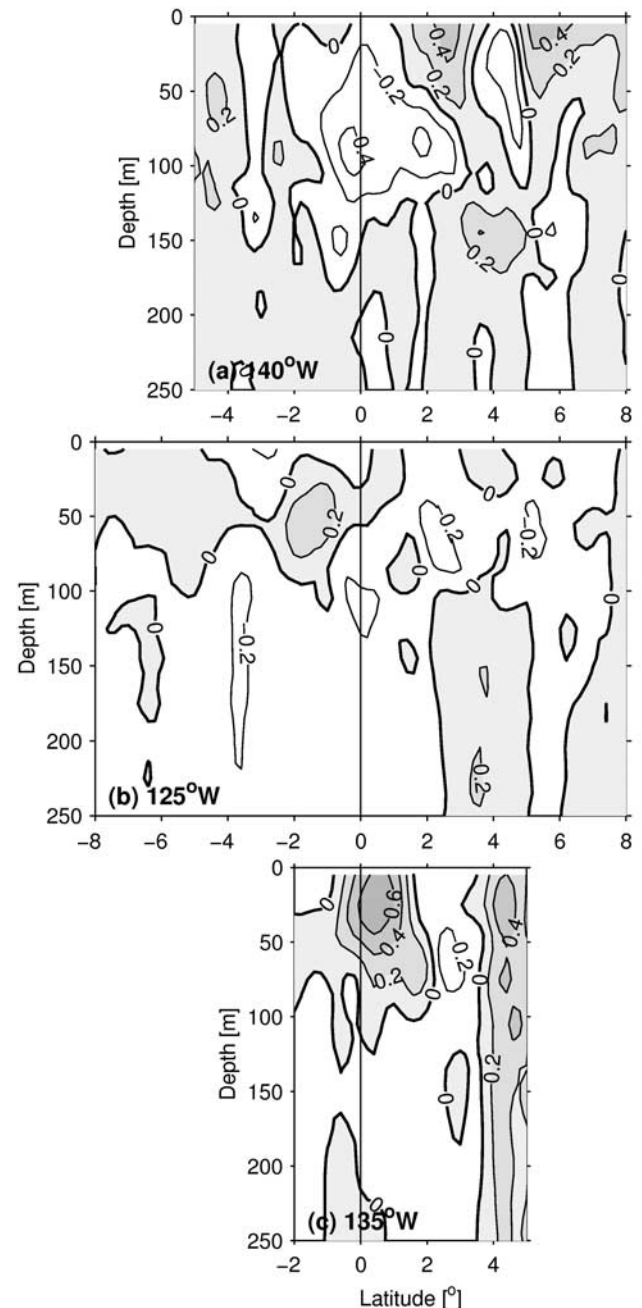


**Figure 3.** Vertical meridional sections of meridional velocity from shipboard ADCP data. Increasingly northward (positive) values are increasingly shaded. Other details follow Figure 2.
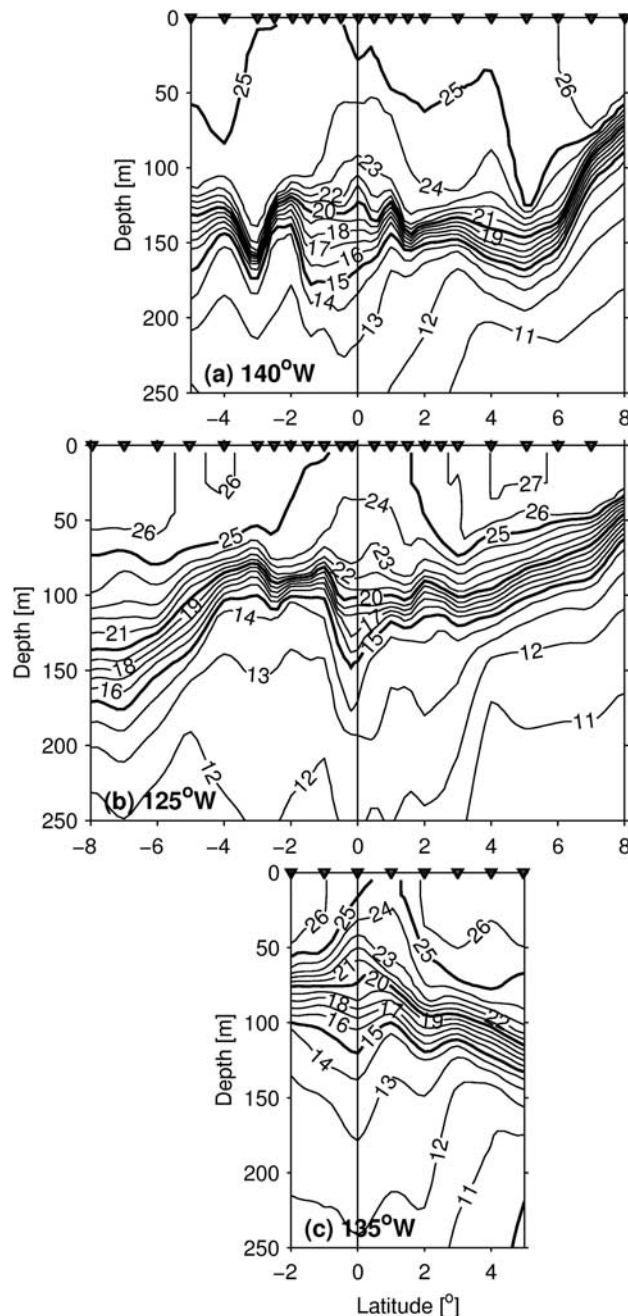
saturated for long, so these features are almost certainly signatures of equatorial upwelling. The displacement of these upwelling signatures in each section is in exactly the sense expected if observed equatorial meridional velocities

**Figure 4.** Vertical meridional sections of potential temperature from CTD data contoured at 1°C intervals against depth and latitude. Isotherms at 5°C intervals are thick. Small triangles along upper edges show CTD station locations. Other details follow Figure 2.

as the northern branch of the SEC and the NECC are on the wane [*Reverdin et al.*, 1994; *Donguy and Meyers*, 1996; *Johnson et al.*, 2002]. February is the start of the season when the cold tongue in the central and eastern equatorial Pacific briefly warms [*Smith and Reynolds*, 1998] and satellite sea surface temperature (SST) data (Figure 7) show that a gradual warming observed during GasEx-2001 is widespread. This warming is coupled with weakening easterly trade winds (not shown), also typical of the seasonal
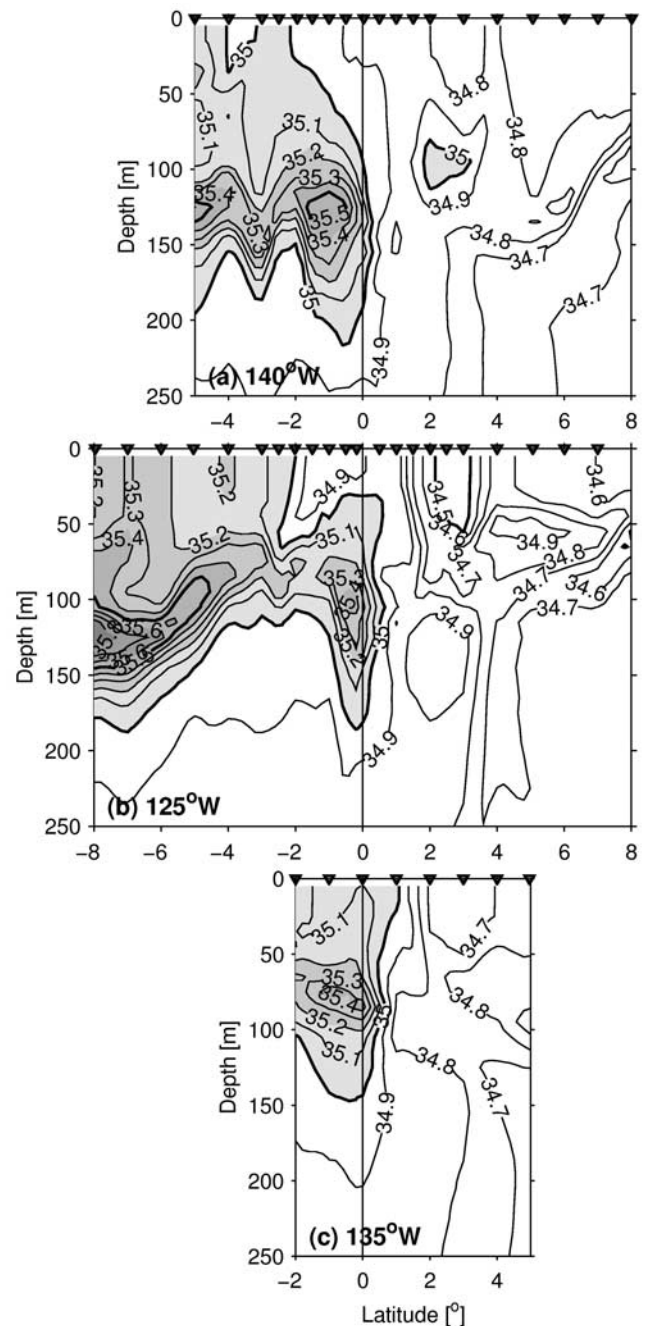


**Figure 5.** Vertical meridional sections of salinity from CTD data contoured at 0.1 (PSS-78) intervals against depth and latitude. Isohalines at 0.5 intervals are thick. Values exceeding 35.0 are increasingly shaded. Other details follow Figure 4.
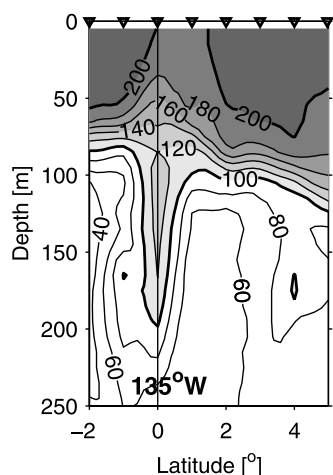
5-month running mean SOI was near 0.5 and falling, consistent with a transition from weak La Niña conditions to normal, so interannual variability is not discussed further.

[16] The most regular perturbation to mean conditions is the seasonal cycle. Normally during February the easterly trade winds weaken in the central Pacific and the thermocline shoals while the cold tongue warms [*Yu and McPhaden*, 1999]. The southern branch of the SEC and the EUC are both relatively weak but strengthening, where-

**Figure 6.** Vertical meridional section of dissolved oxygen from CTD/O$_2$ data contoured against depth and longitude at 20 μmol kg$^{-1}$ intervals. Oxygen isopleths at 100 μmol kg$^{-1}$ intervals are thick. Values exceeding 100 μmol kg$^{-1}$ are increasingly shaded. CTD oxygen was sampled only on the section occupied from 1 to 3 March 2001 nominally along 135°W on the NOAA ship *Ronald H. Brown*. Other details follow Figure 4.

cycle during February. The weakening trades reduce surface cooling and mixing, allowing mixed layer warming.

### 3.3. Kelvin Wave Influences

[17] Winds in the equatorial western Pacific can excite equatorial Kelvin waves, which then propagate rapidly eastward along the waveguide. Kelvin waves have a significant zonal velocity signature, and can change the depth of the equatorial thermocline. These depth changes modify the properties of upwelled water on the equator, as well as modifying the upwelling rate itself. A downwelling Kelvin wave was excited remotely by a strong westerly wind burst in the western equatorial Pacific (extending to 156°E) at the end of November 2000. This feature was followed closely by an upwelling Kelvin wave resulting from the cessation of the westerly wind burst. This disturbance crossed the basin with an eastward phase velocity of around 2 m s$^{-1}$, with downwelling at 125°W commencing at the beginning of January, and upwelling at the beginning of February. The equatorial TAO mooring at 140°W, which provides subsurface measurements of velocity as well as temperature, shows these undulations occurring a few weeks earlier (Figure 8), with the downwelling associated with a strengthened EUC, and the upwelling a weakened EUC, as expected.

[18] With the passage of the upwelling Kelvin wave, the equatorial thermocline steadily shoaled at 125°W during the entire month of February, the time period of GasEx-2001. In the equatorial eastern and central Pacific the equatorial Rossby radius of deformation is around 240 km [*Chelton et al.*, 1998]. Equatorial Kelvin wave thermocline perturbations have a meridional Gaussian decay scaled by twice this radius. Thus the GasEx-2001 experiment, which is no more than 330 km from the equator, lies within the influence of equatorial Kelvin waves. While the array was drifting westward, the rate of 20°C isotherm shoaling at the 2°S,

125°W TAO mooring (35 m over the 28 days of February 2001) is indicative of upwelling on the order of $1.4 \times 10^{-5}$ m s$^{-1}$ during the experiment, a value comparable to mean equatorial rates [*Weisberg and Qiao*, 2000]. However, a vertical migration of isopycnals or isotherms alone implies little about the diapycnal processes important for moving carbon rich waters into the mixed layer.

### 3.4. Tropical Instability Wave Influences

[19] TIWs are another source of variability that must be considered for GasEx-2001. TIW signatures are evident in
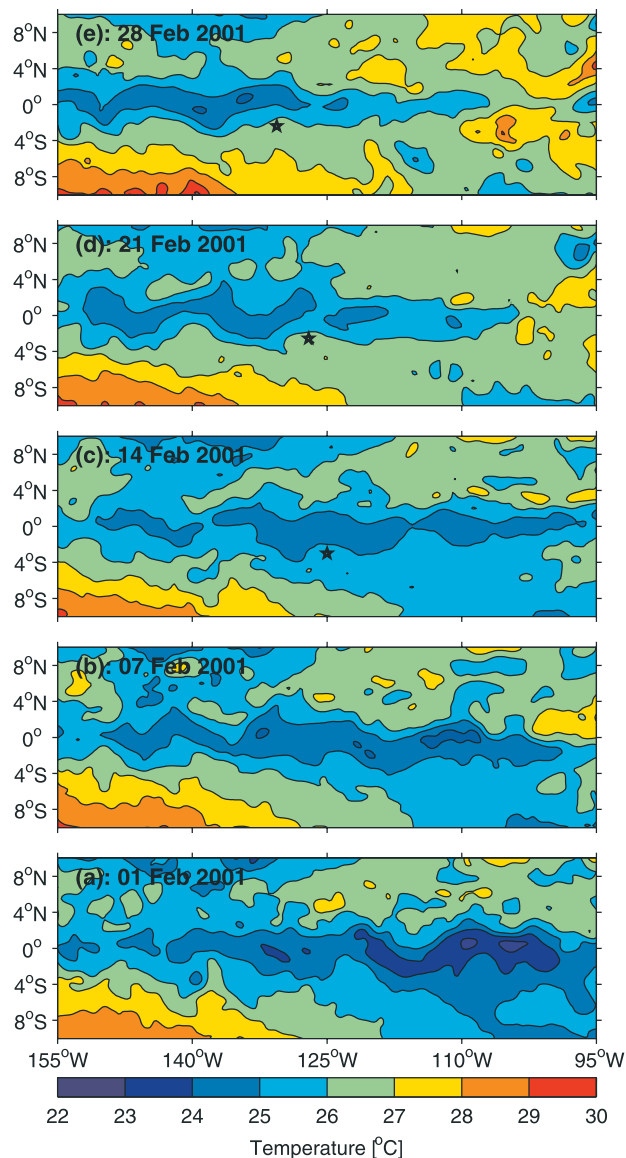


**Figure 7.** Weekly maps from 3-day averages of satellite microwave SST measurements spanning February 2001 in the equatorial Pacific color contoured at 1°C intervals. Data have been smoothed using a two-dimensional quadratic loess smoother [*Cleveland and Devlin*, 1988] with half spans of 2° longitude and 2° latitude for purposes of presentation. (a)–(e) Maps for 3-day periods ending on 1, 7, 14, 21, and 28 February 2001, respectively. Locations of the GasEx-2001 drifting array at temporal midpoints of panels Figures 7c–7e are shown by black pentagrams.
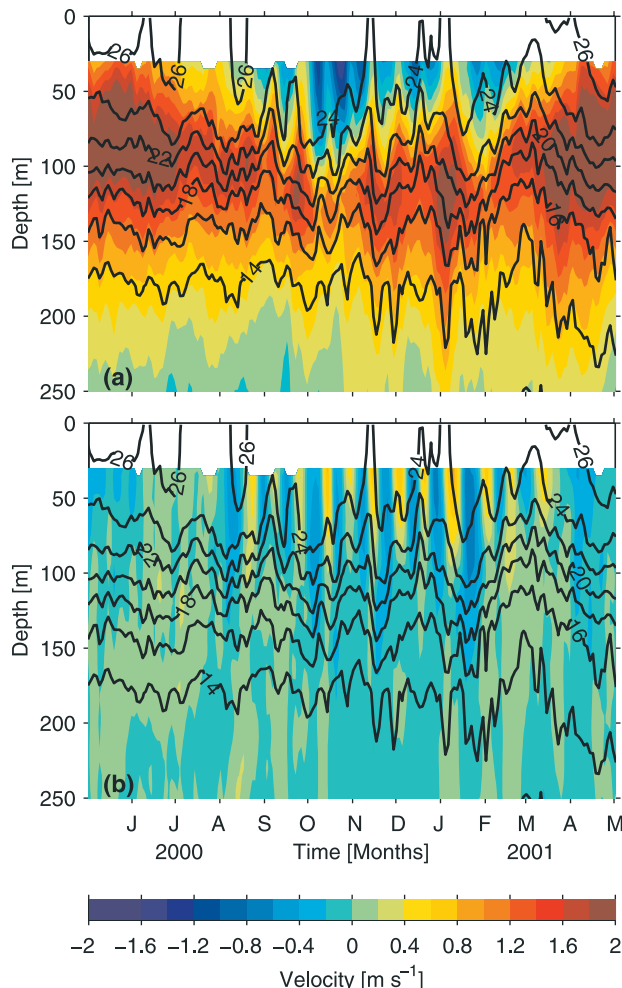
**Figure 8.** Time-depth sections from the equatorial TAO mooring data at 140°W for a year surrounding GasEx-2001 of (a) zonal velocity color contoured at 0.2 m s$^{-1}$ intervals and (b) meridional velocity color contoured at 0.2 m s$^{-1}$ intervals. Potential isotherms at 2°C (thick black lines) are overlaid.

SST and sea surface height (SSH) at 5°N and 2°S [*Chelton et al.*, 2001], as well as in velocity near the equator [*Qiao and Weisberg*, 1995]. They have roughly (within factors of two) a 30 day period, a 1000 km zonal wavelength, and westward phase propagation of about 0.4 m s$^{-1}$ [*Polito et al.*, 2001]. They are most prevalent in the Boreal summer and autumn and during La Niña conditions, when zonal currents from which they gain energy [*Proehl*, 1998] are strong [*Baturin and Niiler*, 1997]. TIW velocities can be of the same magnitude as the mean zonal circulation and overwhelm the mean meridional velocities by an order of magnitude. Thus TIWs can be highly nonlinear [*Kennan and Flament*, 2000], with strong advection, upwelling, frontogenesis [*Johnson*, 1996], and lateral mixing. They thus significantly impact heat budgets [*Swenson and Hansen*, 1999], biogeochemical property distributions such as chlorophyll [*Strutton et al.*, 2001] and presumably $CO_2$ distributions and air-sea exchange. In fact, since TIWs involve strong ocean velocities in an area of weak winds, they can even modulate surface stress [*Polito et al.*, 2001].

Vertical velocities associated with TIWs also overwhelm mean values on the equator [*Weisberg and Qiao*, 2000]. February, when GasEx-2001 was conducted, is a transition time between the boreal spring, when the NECC and north SEC are weak along with the TIWs, and the rest of the year when these currents and the TIWs are strong.

[20] The meridional sections taken during around the time of the experiment suggest TIW activity. First, zonal velocities associated with the NECC and SEC are much stronger at 140°W than at 125°W (Figure 2), and the thermocline trough much deeper (Figure 4), despite the relatively short zonal and temporal separation of these two sections. These differences suggest strong variability over relatively short scales. In addition, as already mentioned, there are strong meridional velocities in these sections (Figure 3), which appear to advect the signatures of equatorial upwelling off the equator (Figures 4–6).

[21] The meridional velocities from the equatorial TAO mooring at 140°W clearly show that TIWs are still present, but fading in February 2001 (Figure 8). Finally, TIW signatures are present in maps of microwave satellite SST data in the region (Figure 7). They can be seen as meridional undulations at the edges of the equatorial cold tongue with a zonal wavelength of about 1500 km and westward phase propagation. The TIWs periodically displace the SST minimum from the equator. The GasEx-2001 array drifts along behind the crest of a TIW. Observations [*Kennan and Flament*, 2000] and ocean general circulation model simulations [*Harrison*, 1996] suggest that location in this phase of the TIW is likely to be associated with strong westward velocities, little meridional velocity, and upwelling.

## 4. Water Mass and Velocity Structure During the Experiment

[22] Here the local temperature, salinity, and horizontal velocity fields are described. The very strong tropical thermocline is found between the warm near-surface layer (temperatures above 26°C) and the equatorial 13°C thermostad (Figure 9a). The thermocline is found between 60 m and 95 m at the start of the experiment. By the end of the experiment the thermocline is located between about 50 m and 85 m. The two intensive sampling periods near year-days 47 and 57 reveal some short timescale variability in thermocline depth. This variability is likely owing to a variety of sources including internal waves and tides. The daily CTD casts do not resolve this variability, so trends over a few casts (such as the apparent thermocline deepening over the last few days of the experiment) may simply be aliased short-term variability. Hence only an overall shoaling rate can be estimated safely from the time series. To make this estimate, linear fits to depths of a set of potential isopycnals within the thermocline are made against time. These depths are found from the 29 CTD/O$_2$ casts occupied along the course of the array drift path (Figure 1, circles and crosses), excluding casts taken far from the array during the regional butterfly surveys. This analysis suggests that the thermocline shoals about 13(±8) m over 15 days, or 1.0(±0.6) × 10$^{-5}$ m s$^{-1}$, following the mostly westward array drift of 715 km during that time. The uncertainties are 95% confidence limits for the fits assuming each cast is statistically independent. Upwelling rates are very similar
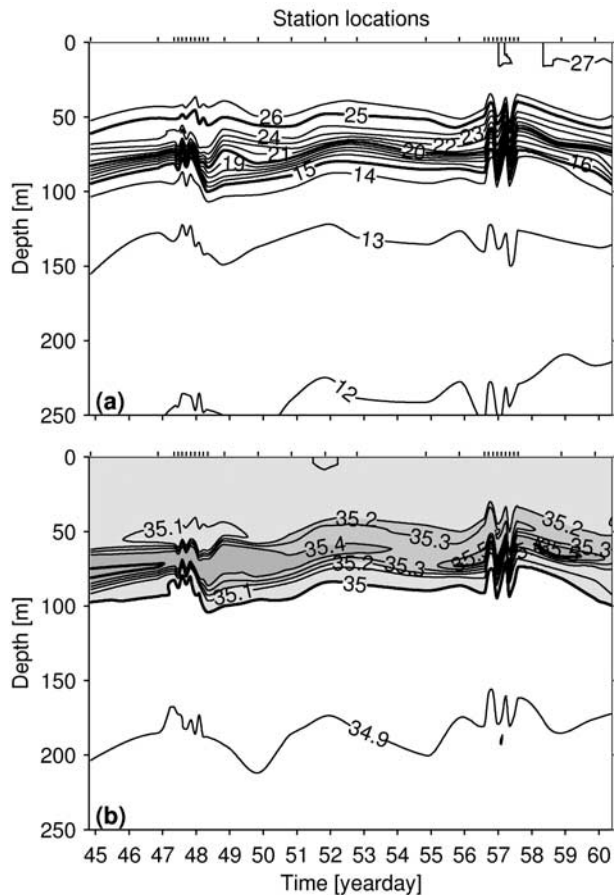
**Figure 9.** Vertical temporal sections of data from CTD/O$_2$ casts occupied along the instrument array drift (Figure 1, circles and crosses) contoured against time (yearday) and depth (m). (a) Potential temperature (θ) contoured at 1°C intervals, with thick isotherms at 5°C intervals. (b) Salinity contoured at 0.1 (PSS-78) intervals with thick isotherms at 0.5 intervals. Values exceeding 35.0 are increasingly shaded. Data have been vertically filtered with a 9-dbar Hanning filter for clarity of presentation. Ticks along the top axis show station times.

for all isopycnals within the thermocline and well within the range of short timescale variability in upwelling on the equator [*Weisberg and Qiao*, 2000].

[23] The most pertinent feature in the salinity field (Figure 9b) is the salinity maximum embedded within the tropical thermocline. This maximum originates in the southern subtropics in a region of high evaporation and is advected equatorward within the SEC [*Tsuchiya*, 1968]. This distinctive signature of mean equatorward flow within the thermocline contrasts with the fresher water above that is advected poleward in the mean by the near-surface flow [*Poulain*, 1993].

[24] Zonal velocity during the experiment is surface intensified and westward (Figure 10a), as expected in the SEC [*Wyrtki and Kilonsky*, 1984]. The zonal velocity at 25 m builds from near $-0.2$ m s$^{-1}$ to $-0.6$ m s$^{-1}$ during the course of the experiment. Mean westward flow during the experiment increases monotonically from 450 to 17 m. The strongest vertical shear of zonal velocity is found in

the thermocline, suggesting the likely importance of geostrophy. However, vertical shear associated with surface intensification of westward velocity persists above the thermocline. Since easterly trades are predominant through the experiment, this near-surface vertical shear in zonal velocity, together with the meridional velocity structure described below, is suggestive of the role of Ekman dynamics [*Price et al.*, 1987].

[25] Like the zonal velocity, meridional velocity is weak below the thermocline, but it does not increase monotonically toward the surface (Figure 10b). Meridional velocity is increasingly northward up to the top of the thermocline, with strong vertical shear found within the thermocline. However, a reversal in the sign of this shear above the thermocline creates a clear maximum in northward flow that lies near the top of the thermocline. This maximum in northward flow is consonant with the salinity maximum
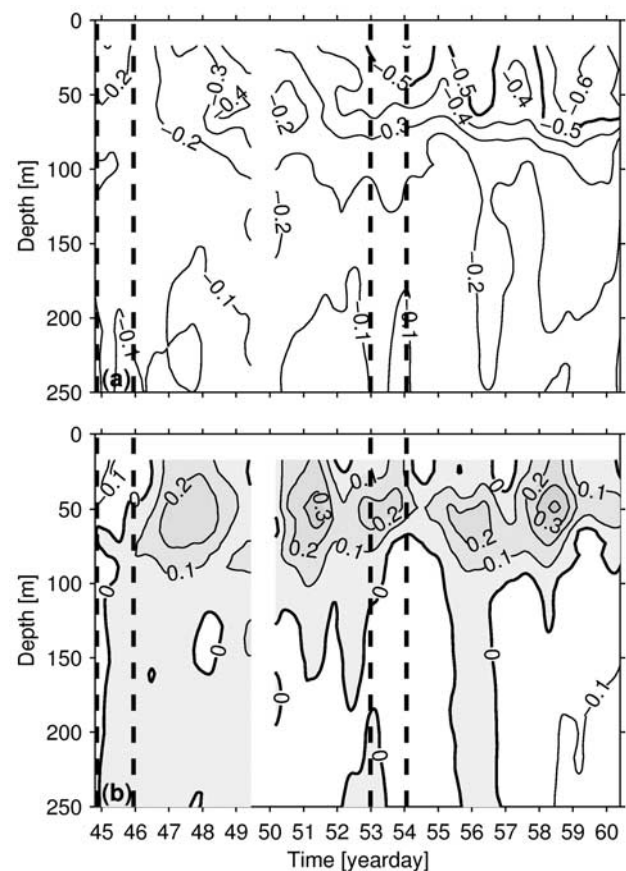


**Figure 10.** Vertical temporal sections of (a) zonal velocity and (b) meridional velocity contoured at 0.1 m s$^{-1}$ intervals against time (yearday) and depth (m) with positive (eastward and northward, respectively) values increasingly shaded and thick values at 0.5 m s$^{-1}$ intervals. The data are smoothed temporally using a low-pass filter with a 24-hour half-power point for clarity of presentation. A data gap of 18 hours starting during yearday 49 is left uncontoured. Unlike Figure 9, data taken during the regional butterfly surveys are included. These surveys (delimited by thick dashed vertical lines around days 45 and 53) take about a day and range as far as 80 km from the drift of the instrument array.
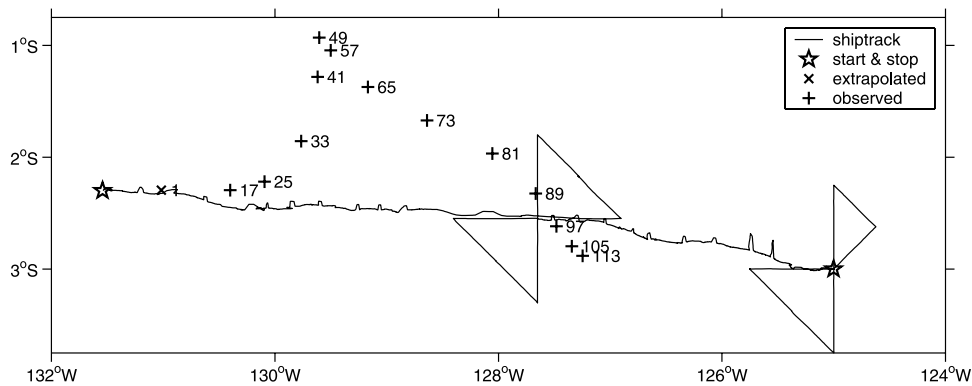
**Figure 11.** Displacement diagram made by integrating observed ADCP velocities at observed depths over the 15.5-day course of the experiment (pluses with depths labeled) with the ship track over the course of the experiment (solid line) from initial deployment of the drifting instrument array to final recovery (stars) shown for reference. The 18-hour gap in ADCP velocities during yearday 49 (Figure 10) is filled by linearly interpolation. A surface displacement (cross with depth labeled) is estimated as detailed in the text.

found within the thermocline being advected northward from its southern subtropical source. By 17 m, the shallowest ADCP observation depth, the northward flow is much weaker in the mean, and occasionally reverses sign. The vertical shear of meridional velocity is also quite weak by 17 m. This tendency toward near-surface flow to the left (looking downwind of the easterly trades, and relative to the northward flow at the top of the thermocline), together with the zonal velocity structure described above, may suggest the importance of Ekman dynamics.

[26] Lateral density gradients within the mixed layer estimated from the local butterfly surveys are about a tenth of the size needed to support the observed near-surface vertical shear of horizontal velocity through the thermal wind relation (geostrophy). This discrepancy adds support to the likely importance of Ekman dynamics in setting the near-surface velocity structure. In addition, mean vertical shear of horizontal velocity (not shown) from the PWP model run below, which contains nothing but midlatitude wind-driven dynamics, agrees well observed mean shear values from the ADCP over depths between 17 and 49 m.

[27] Integration of the observed hourly averages of near-surface ADCP velocities over the course of the 15.5-day experiment to infer displacements at various depths during the experiment (Figure 11) quantifies the magnitude of the vertical shear of horizontal velocity. The large shear in the thermocline (between 105 m and 49 m) leads to increasing west-northwestward displacements with decreasing depth, and is likely largely geostrophic. However, above the thermocline (between 49 m and 17 m), the downwind (mostly westward) shear is reduced, and the displacements abruptly shift southward with decreasing depth, to the left of the (westward) wind stress (relative to the direction of presumably geostrophic flow within the thermocline) under the influence of Ekman dynamics. The vertical shear of horizontal velocity within the mixed layer would bring water at the mixed layer base (say 33 m) northeastward by about 86 km relative to water nearer the surface (the shallowest observed values at 17 m). This significant upper ocean vertical shear of horizontal velocity within the mixed layer may be important for mixed layer budgets of heat and carbon, as discussed below.

[28] The 17-m integrated displacement from the ADCP velocities falls about 127 km short of the mostly westward 731-km drift of the instrument array (Figure 11). Thus the array appears effectively drogued at some depth above 17 m. The mean vertical shears of horizontal velocities in the upper ocean below 17-m and over the entire mixed layer for the PWP model run presented below suggest that linear extrapolation of observed vertical shear of zonal velocity between the two shallowest ADCP measurement bins at 17 m and 25 m and assuming meridional velocity observed at 17 m stays constant to the surface should give a reasonable prediction of displacement at 1-m depth (Figure 11). This prediction is only about 60 km to the east of the final instrument array location. Given this shortfall, it is plausible that windage from the easterly trades on the array pushed it westward in relation to even the near-surface flow, so that the array was not truly Lagrangian at any depth. Given the uncertainty in extrapolating displacements from observed values to the surface, the array and the integrated near-surface flow measurements are in reasonable agreement. However, the discrepancy that remains could also be of importance for mixed layer heat, carbon, nutrient, and oxygen budgets, and its potential effects are discussed below.

## 5. Mixed Layer Model

[29] To investigate the effects of entrainment at the mixed layer base on water property budgets, a simple one-dimensional mixed layer model (PWP) is run. The model is initialized with temperature and salinity profiles from the CTD/$O_2$ station occupied at the start of the experiment (Figure 1, eastmost circle) and then forced for 15 days from the start of yearday 45 through the start of yearday 60 using heat, freshwater, and momentum fluxes estimated from shipboard meteorological measurements. The model domain extends from the surface to 500 m at 1-m intervals, and the model time step is set to 30 min, matching the averaging interval for the meteorological forcing.

[30] The weather during the core 15 days of the experiment was typically tropical. The wind was low, 6.0(±1.3) m s$^{-1}$, (mean and standard deviation) and generally came from slightly south of east. About 6 cm of rain fell, mostly during yearday 51. Diurnal peaks in downwelling solar radiation ranged from 820 to 1060 W$^{-2}$. Given the long inertial period at the very low latitudes of GasEx-2001, initial transients are very difficult to avoid without artificially reducing observed winds during the first part of the experiment. As a compromise between inducing transients and imposing artificially low winds for too long, wind stresses are ramped up linearly from zero to observed values over the first three hours of the run.

[31] Water type Jerlov IB, with a shortwave attenuation depth of 17 m, is usually assumed to be typical of equatorial regions for the purposes of energy absorption [Schudlich and Price, 1992]. However, analysis of chlorophyll concentrations from the cruise following Morel and Maritorena [2001] results in a 25-m shortwave attenuation depth [Strutton et al., 2004], so that value is used here. This substitution helps close the mixed layer heat budget.

[32] Several modifications are made to the conventional PWP configuration. First, a weak background vertical diffusivity well below thermocline values [Gregg, 1998] is added, k$_z$ = 1 × 10$^{-6}$ m$^2$ s$^{-1}$. While this addition has little effect over the 15-day integration, it adds realism. Second, surface freshwater fluxes are applied and salinity is treated as an active variable. Third, biogeochemical constituents, including DIC, O$_2$, NO$_3$, and PO$_4$, are added and carried along in the model as passive tracers to investigate the role of entrainment in the mixed layer budgets for carbon, oxygen, and nutrients in the absence of biological effects and air-sea gas exchange. However, neglect of the source and sink terms for these biogeochemical constituents may bias model estimates of entrainment on their mixed layer concentrations. Fourth, the full equation of state (EOS-80), rather than a linearized one more typical of PWP models, is used to calculate potential density and potential temperature, θ. Fifth, in one of the two model integrations presented, a vertical velocity profile is prescribed with a maximum value of w = 1.0 × 10$^{-5}$ m s$^{-1}$. This value is estimated from the thermocline shoaling of 13 m over 15.5 days as previously discussed. In the model w is assumed to increase linearly from zero at the surface to a maximum at the base of the mixed layer (defined in the model as the depth to which mixing occurs) and then to decrease again to zero at the maximum model depth of 500 m. This simple upwelling pattern is expected from Ekman divergence in the mixed layer [Schudlich and Price, 1992]. Effects of the small horizontal convergence below and divergence above the mixed layer are neglected in the model.

[33] To estimate an initial high vertical resolution DIC profile, a multiple linear regression of DIC [Goyet and Davis, 1997] is made on θ, salinity, apparent oxygen utilization, and unity (the latter allows a constant offset), using all the bottle data flagged as "good" from all the stations following the instrument array drift (Figure 1, circles and crosses). The fit is done iteratively, discarding bottle data with residual magnitudes exceeding 2.8 times the residual standard deviation until no more data are discarded. The iterations remove a few outlying values from the fit.
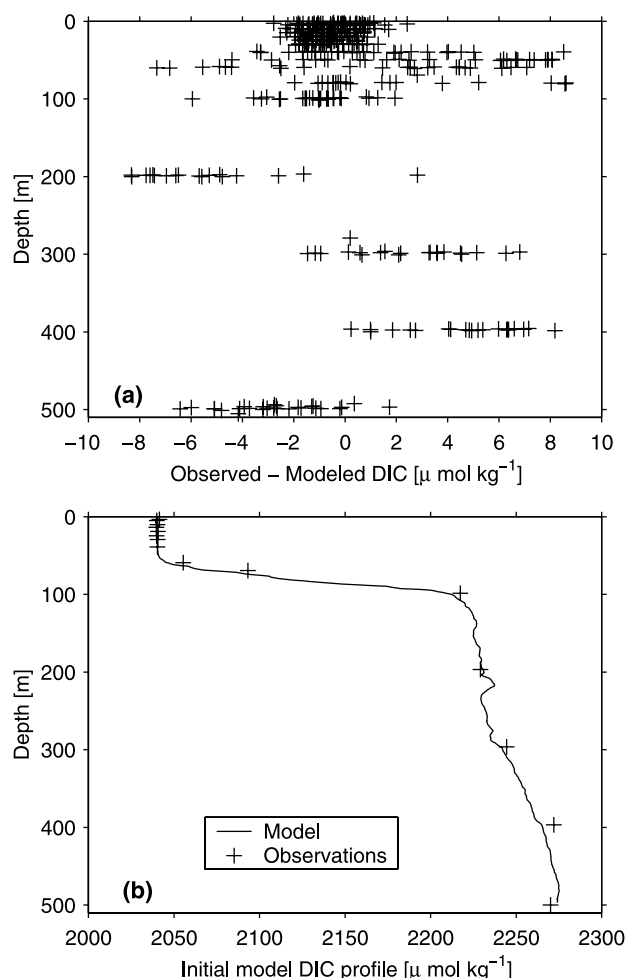


**Figure 12.** (a). Residuals (observations—model) of dissolved inorganic carbon (DIC; μmol kg$^{-1}$) for a multiple linear regression described in the text plotted against depth (m). (b). Initial model high-resolution profile of DIC (solid line) plotted against depth constructed by applying the regression parameters to data from the first CTD/O2 station along the instrument drift track. DIC bottle data from that same station (pluses) are in good agreement with the initial model profile.

Residuals of the 406 values which remain (95% of the initial 428) show only slight structure versus depth (Figure 12a). The final standard deviations of these residuals is only 3.1 μmol kg$^{-1}$, which is not much larger than the precision of the measurement. The resulting fit coefficients are applied to data from the initial 1-dbar vertical resolution CTD/O$_2$ profile to obtain a high-resolution DIC profile which agrees well with the DIC bottle data for that profile (Figure 12b). This high-resolution DIC profile is used to initialize the PWP model.

[34] This same process is followed to obtain high-resolution NO$_3$ and PO$_4$ profiles. For the former, 355 out of the 381 bottles flagged good (91%) are retained in the final fit, which has a standard deviation of 0.5 μmol kg$^{-1}$. For the latter, 298 out of the 334 bottles flagged good (89%) are retained in the final fit, which has a standard deviation of 0.03 μmol kg$^{-1}$. These standard deviations correspond to
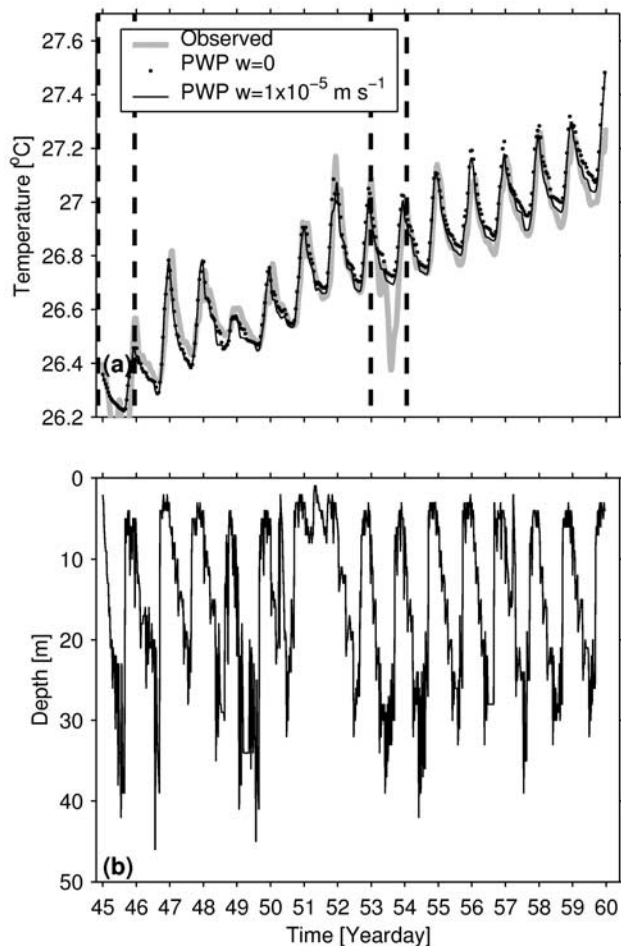
**Figure 13.** (a) Shipboard sea surface temperature (SST, °C) plotted versus time (thick shaded line). Data are smoothed using a low-pass filter with a 3-hour half-power point for clarity of presentation. Identically smoothed SSTs from PWP model integrations without (dotted line) and with (thin black line) prescribed upwelling are shown for comparison. Regional surveys when the ship departs from the drifting instrument array are delimited with thick dashed vertical lines around days 45 and 53. (b) Modeled mixed layer depth from the integration with prescribed upwelling plotted versus time with no smoothing.

the measurement precisions, suggesting good fits to the data. The high-resolution $O_2$ profile is obtained directly from the CTD/$O_2$ data.

[35] Of course the mixed layer properties, especially temperature, exhibit significant diurnal variability owing to daily cycles in surface fluxes (PWP), and GasEx-2001 is no exception. Thus the daily noon CTD/$O_2$ stations, and even the data from the two CTD/$O_2$ time series, are not sufficient to evaluate the model performance for diurnal timescales. Hence the more rapidly sampled shipboard sea surface temperature (SST) is employed in this capacity. When the observed SST is compared with model results (Figure 13a), there is initial agreement as should be expected, but the model temperatures rise more quickly than the observed values. By yearday 59.65 the disagreement during the (night) time of coldest SST is around 0.1°C

for the model run without upwelling. (Using the Jerlov IB 17-m shortwave attenuation depth instead of the 25-m value suggested by the chlorophyll data worsens agreement to 0.2°C). For the model run with upwelling, the disagreement is reduced to about 0.04°C. This remaining difference between modeled and observed SST could easily be accounted for by a surface heat flux bias well below the estimated accuracy of 10 W m$^{-2}$.

[36] Every day the mixed layer depth of the model with upwelling (Figure 13b) shoals to between 1 and 4 m (most frequently 3 m) in the late afternoon, because of the accumulated effects of near-surface daytime warming on the stratification. Every day the model mixed layer depth is greatest, reaching between 8 m and 46 m on any given day, in the early morning, after nighttime cooling and subsequent mixing. The most frequent maximum nocturnal mixed layer depth (the mode) is 32 m. Like the diurnal cycle in SST, this diurnal cycle in mixed layer depth is typical (PWP). The model without upwelling (not shown) exhibits very similar behavior in mixed layer depth.

[37] To qualitatively evaluate the overall evolution of the vertical structure of the model, temperature profiles are extracted from the model at the times near the start and end of the integration when CTD/$O_2$ stations were occupied. The initial profiles are in exact agreement (Figure 14) since the model is initialized using the CTD/$O_2$ profile. The observed profile occupied at yearday 58.89, close to the end the experiment and the integration, compares well with the corresponding model profile. Both reveal a thermocline that has shoaled about 13 m. In the model this shoaling is a direct result of the prescribed upwelling. Since the upwelling rate was estimated from the CTD/$O_2$ observations, the agreement is to be expected. Small vertical-scale features visible in all the observed profiles and the initial model profile are not present in the later model profiles. These features have been smoothed out by the background vertical diffusion. Observed and modeled temperatures above the thermocline are also in fairly close agreement. While only
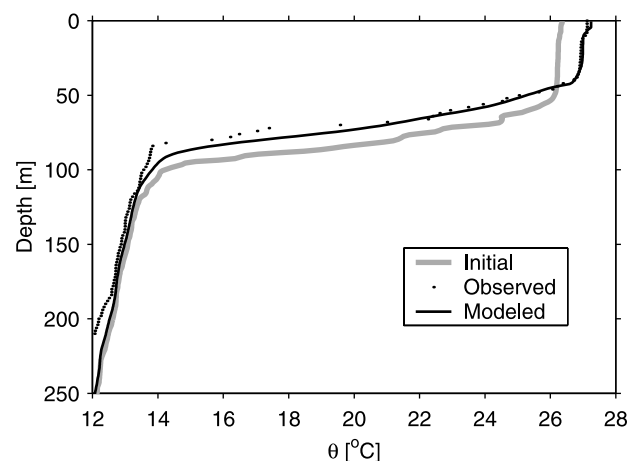


**Figure 14.** Initial observed and modeled potential temperature (θ, °C) profiles versus depth (m) exactly overlap since the model is initialized with observations (thick shaded line). The observed θ profile taken at yearday 58.89 (dotted line) is also in good agreement with the corresponding model θ profile (thin black line).
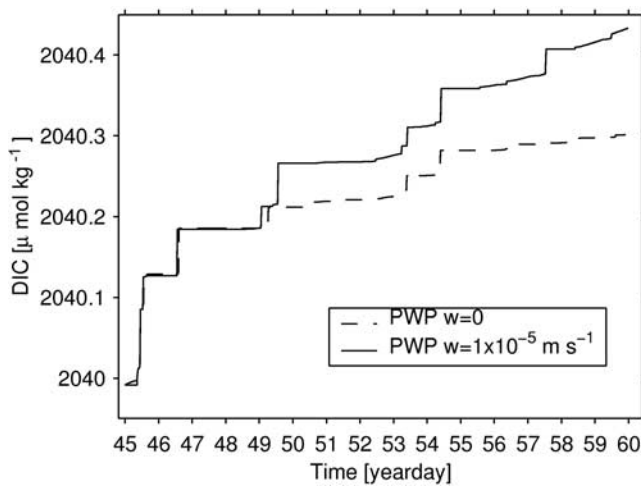
**Figure 15.** Modeled dissolved inorganic carbon (DIC, $\mu$mol kg$^{-1}$) averaged over the top 30 m of the water column for the model runs without (dashed line) and with (solid line) upwelling plotted versus time.

just discernible given the large temperature scale in the plot, temperature observations above the thermocline are cooler than the model by roughly 0.05°C, with a local noon difference slightly larger than the early morning difference already discussed for the SST record. Thus the gross modeled upper ocean structure agrees well with the observations over the course of the experiment. This agreement, as stated above, lies well within the likely uncertainty of measured surface heat fluxes.

[38] Given the success in modeling the observed upper ocean heat budget, we are emboldened to examine the effects of mixed layer entrainment on the DIC budget through the temporal evolution of modeled DIC in the upper 30 m (Figure 15). This averaging depth is chosen as typical of the maximum nocturnal mixed layer depth from examination of observed upper ocean profiles and the model results. For the model run without upwelling the mixed layer DIC increases about 0.3 $\mu$mol kg$^{-1}$ over the course of the experiment. For the run with upwelling, mixed layer DIC increases about 0.4 $\mu$mol kg$^{-1}$ over the course of the experiment. The inclusion of upwelling slightly enhances entrainment of deeper carbon-rich water into the mixed layer. The effects of entrainment during the first night of both model runs are larger than for the rest of the runs, possibly because of spurious initial model transients. As a result, the model estimates of the effect of entrainment on the mixed layer carbon budget may be biased high. The step-like increases in near-surface DIC result from entrainment of DIC-rich water from below, and are associated with unusually deep nocturnal mixed layers (Figure 13).

[39] The corresponding calculations for $O_2$, $NO_3$, and $PO_4$, using output from the PWP model with prescribed upwelling, suggest mixed layer enrichments of 0.3 $\mu$mol kg$^{-1}$, 0.04 $\mu$mol kg$^{-1}$, and 0.005 $\mu$mol kg$^{-1}$, respectively for these quantities. The most unexpected of these results is for oxygen, because the equatorial thermostad is oxygen-poor so one would anticipate that entrainment would decrease mixed layer oxygen values. However, there is a slight increase of oxygen from the surface to a subsurface maximum near 50–60 m, and it is entrainment of water from these depths that results in a mixed layer oxygen enrichment.

## 6. Differential Horizontal Advection and Array Slippage Within the Mixed Layer

[40] Two effects not included in the simple 1-D model require estimates of horizontal property gradients to estimate their magnitudes. Two local butterfly surveys were completed around the floats as they drifted west, one immediately after the floats were deployed during yearday 45 and a second midway through the experiment during yearday 53 (Figure 1, stars). The meridional and zonal gradients for various property values from those surveys (Table 1) are estimated by fitting $x$-$y$ planes to the data, first shifting the locations of stations to lie around an origin at the center of each survey, and also allowing constant offsets of water properties between the two surveys. Reported errors are 95% confidence limits estimated from chi squares and a Student's $t$ test assuming 10 degrees of freedom (a four-parameter fit applied to data from 14 distinct geographic locations). For $\theta$, 30-dbar values are used, a depth chosen to be within the mixed layer but below the effects of diurnal heating. For the other water properties, values above 32 dbar are used. The errors for the gradients are generally comparable to the gradients themselves.

[41] One potential influence not included in the PWP model is that of differential horizontal advection within the mixed layer (Figure 11). Waters near the base of the mixed layer (33 m) move substantially east-northeast relative to the surface (1 m) water over the experiment duration. The differential meridional displacement of the observed displacement at 33 m is about 49 km northward over the course of the experiment relative to the extrapolated displacement at 1 m. The corresponding differential zonal displacement is about 138 km eastward over the 15.5 days.

[42] Applying mixed layer water property gradients estimated from the two regional butterfly surveys (Table 1) to the lateral displacements estimated from the ADCP velocity data above and dividing by two (to account for two end-member vertical mixing) allows estimates of the potential effects of differential lateral advection within the mixed layer owing to vertical shear of horizontal velocity there (Table 2). Gradients are estimated by a planar fit to the data that allows for an offset in properties between butterfly surveys, and assuming that data from each station are independent. The 95% confidence limits given are based

**Table 1.** Meridional and Zonal Gradients of Potential Temperature ($\theta$) at 30 dbar and Other Water Property Measurements Made Above 32 dbar as Estimated From the Two Regional Butterfly Surveys Taken During Days 45 and 53 With 95% Confidence Limits

| Water Property Gradient | Zonal | Meridional |
|---|---|---|
| $\nabla\theta$, $10^{-3}$ °C km$^{-1}$ | 0.0 ($\pm$2) | $-2$ ($\pm$2) |
| $\nabla$DIC, $\mu$mol kg$^{-1}$ km$^{-1}$ | 0.02 ($\pm$0.04) | $-0.08$ ($\pm$0.04) |
| $\nabla O_2$, $\mu$mol kg$^{-1}$ km$^{-1}$ | $-0.003$ ($\pm$0.007) | 0.001 ($\pm$0.007) |
| $\nabla NO_3$, $\mu$mol kg$^{-1}$ km$^{-1}$ | 0.001 ($\pm$0.004) | $-0.010$ ($\pm$0.004) |
| $\nabla PO_4$, $\mu$mol kg$^{-1}$ km$^{-1}$ | 0.0001 ($\pm$0.001) | $-0.0004$ ($\pm$0.0002) |

**Table 2.** Estimates of Some Effects on Mixed Layer Properties With Gradient Estimate–Based 95% Confidence Limits Where Applicable[a]

| Water Property | Mixed Layer Entrainment | Differential Advection | Slippage | Total |
|---|---|---|---|---|
| $\theta$, °C | n/a | 0.04 (±0.14) | −0.00 (±0.11) | 0.04 (±0.18) |
| DIC, $\mu$mol kg$^{-1}$ | 0.4 | 0.7 (±3.1) | −1.0 (±2.6) | 0.1 (±4.0) |
| $O_2$, $\mu$mol kg$^{-1}$ | 0.3 | 0.2 (±0.5) | 0.2 (±0.4) | 0.7 (±0.6) |
| $NO_3$, $\mu$mol kg$^{-1}$ | 0.04 | 0.1 (±0.3) | −0.1 (±0.2) | 0.04 (±0.4) |
| $PO_4$, $\mu$mol kg$^{-1}$ | 0.005 | 0.0007 (±0.013) | −0.007 (±0.008) | −0.001 (±0.015) |

[a]Air-sea heat fluxes have been included in the mixed layer model, and the effects of mixed layer entrainment on $\theta$ have not been isolated.

on the errors in the property gradient estimates alone, and assume the vertical shear of horizontal velocity within the mixed layer (including extrapolation of displacements observed below 17 m to the surface as detailed above) is known exactly. The vertical shear is probably better known than the property gradients, even including extrapolation errors, but uncertainty in the shear, if accounted for in the error estimates, would increase them further. Nonetheless this calculation suggests that differential advection would tend to inject warm carbon, nutrient, and oxygen-rich subsurface waters from the east-southeast under the surface waters. The temperature change tends to slightly increase the disagreement between observed and modeled SST, although the sign is uncertain given the error bars. For DIC, oxygen, and nutrients the differential advective effects result in mixed layer enrichments of similar size to the entrainment at the mixed layer base (Table 2). All have large uncertainties, but they do give some indication of the potential magnitude of the effect of differential horizontal advection within the mixed layer on mixed layer property budgets.

[43] Another potential effect on the mixed layer properties observed by the drifting instrument array is the possibility that the array may not have exactly followed the surface waters (slippage), as discussed above. A comparison of the end point of the array and the displacement based on integration of ADCP velocities linearly extrapolated to 1-m depth (Figure 11) suggests that the array finished about 58 km due west of the surface displacements. There is no regional survey at the conclusion of the experiment to assess the local gradients at that time and location. However, application of these distances to the surface gradients (Table 1) estimated from the two prior butterfly surveys suggests that the instrument array mixed layer at the end of the experiment may have been DIC and nutrient richer, but oxygen poorer (Table 2) than it would have been if the array were exactly following the surface waters. Again, the large uncertainties in these differences only incorporate uncertainties in the gradient estimates, and assume the slippage is known exactly. The slippage may be better known than the gradients, even with extrapolation, but its uncertainty, were it known, would increase the error estimates.

## 7. Discussion

[44] A typically complex mix of ocean phenomena influenced large-scale oceanographic conditions during GasEx-2001. The experiment was conducted just south of the equator in the Central Pacific during the second half of February 2001. The zonal system of equatorial currents was observed to be within a normal range, as might be expected given the near normal phase of the SOI for the time period. Of particular relevance, the southern branch of the SEC advected the drifting array primarily westward, as expected. Water property distributions were also fairly typical. In particular, upwelling signatures were evident in chimneys of cold, salty, oxygen-poor water extending up into the mixed layer near the equator. This upwelling supplies the carbon-rich water to the surface, making the equatorial Pacific a region of strong outgassing. The expected effects of the seasonal cycle, the weakening trade winds, shoaling thermocline, and most particularly the warming mixed layer temperatures all influenced conditions during the experiment. Most notably, this seasonal cycle resulted in significant warming of the mixed layer during GasEx-2001.

[45] More transient phenomena also influenced conditions during GasEx-2001. A remotely forced downwelling Kelvin wave followed immediately by an upwelling Kelvin wave passed by the experiment location in early February. The influence of the upwelling Kelvin wave during GasEx-2001 quite likely overwhelmed any thermocline deepening that would be expected during the westward drift of the array. The sum of these effects likely contributed to the slowly shoaling thermocline observed during the experiment. In addition, while TIWs were weakening in strength, they were still present and influential during GasEx-2001. Analysis of satellite SST data suggest the drifting array was following the crest of a TIW. This position could help account for the rapid westward drift of the array. In addition, TIWs are associated with strong vertical velocities, and GasEx-2001 appears to have been conducted in phase of the TIW conducive to strong westward flow and off-equatorial upwelling.

[46] A PWP mixed layer model, initialized with CTD/$O_2$, DIC, and nutrient observations, run with surface fluxes estimated from shipboard meteorological forcing, and using a shortwave attenuation depth derived from chlorophyll data, agrees fairly well with subsequent CTD/$O_2$ and SST observations, with the model trending slightly warmer than the observations over the course of the run. Agreement is improved to well within the uncertainties of the heat fluxes forcing the model by prescribing upwelling (estimated from observed thermocline shoaling) in the model. The upwelling obviously brings more cold water into the mixed layer, reducing model temperatures in the mixed layer. Since colder water is more carbon-rich, the upwelling also brings slightly more carbon (as well as nutrients and oxygen) into the mixed layer. The end result is a net increase in DIC of about 0.4 $\mu$mol kg$^{-1}$ within the mixed layer over 15 days.

Other effects not accounted for in the one-dimensional model (aside from biology and gas exchange) might also be important in the mixed layer property budgets. These include differential horizontal advection within the mixed layer, slight departures from a Lagrangian experiment by array slippage (Table 2), and horizontal divergence associated with the prescribed upwelling profile.

[47] In summary, vertical entrainment at the base of the mixed layer likely slightly enriches the mixed layer with DIC (as well as nutrients and oxygen) over the course of GasEx-2001. Differential horizontal advection within the mixed layer may have effects of the same sign and similar magnitudes on the mixed layer properties, although uncertainties are large. In addition, the slightly non-Lagrangian character of the drifting instrument array may mean that it finished in slightly DIC (and nutrient) poorer water than it might have had it followed a surface water parcel. The sum of these three terms, however, only results in an $0.1(\pm 4.0)$ $\mu$mol kg$^{-1}$ change in DIC. This net change is a very small value. However, the uncertainty is larger than the precision of individual measurements. The reduction of mixed layer DIC observed, on the order 6 $\mu$mol kg$^{-1}$, is significantly larger than the sum of changes because of the physical oceanographic processes considered here. Thus other effects (e.g., biology, air-sea gas exchange, etc.), which are discussed elsewhere in this special issue [e.g., *Sabine et al.*, 2004] appear to be dominant processes in the mixed layer carbon budget during GasEx-2001.

# References

Baturin, N. G., and P. P. Niiler (1997), Effects of instability waves in the mixed layer of the equatorial Pacific, *J. Geophys. Res.*, *102*, 27,771–27,793.

Bryden, H. L., and E. C. Brady (1985), Diagnostic model of the three-dimensional circulation in the upper equatorial Pacific Ocean, *J. Phys. Oceanogr.*, *15*, 1255–1273.

Chavez, F. P., P. G. Strutton, G. E. Friederich, R. A. Feely, G. Feldman, D. Foley, and M. J. McPhaden (1999), Biological and chemical response of the equatorial Pacific Ocean to the 1997–1998 El Niño, *Science*, *286*, 2126–2131.

Chelton, D. B., R. A. deSzoeke, M. G. Schlax, K. El Nagger, and N. Siwertz (1998), Geophysical variability of the first baroclinic Rossby radius of deformation, *J. Phys. Oceanogr.*, *28*, 433–460.

Chelton, D. B., F. J. Wentz, C. L. Gentemann, R. A. de Szoeke, and M. G. Schlax (2001), Satellite microwave SST observations of transequatorial tropical instability waves, *Geophys. Res. Lett.*, *27*, 1239–1242.

Cleveland, W. S., and S. J. Devlin (1988), Locally weighted regression: An approach to regression analysis by local fitting, *J. Am. Stat. Assoc.*, *83*, 596–610.

Delcroix, T., C. Henin, V. Porte, and P. Arkin (1996), Precipitation and sea-surface salinity in the tropical Pacific Ocean, *Deep Sea Res., Part I*, *43*, 1123–1141.

Donguy, J.-R., and G. Meyers (1996), Mean annual variation of transport of major currents in the tropical Pacific Ocean, *Deep Sea Res., Part I*, *43*, 1105–1122.

Feely, R. A., R. Wanninkhof, T. Takahashi, and P. Tans (1999), Influence of El Niño on the equatorial Pacific contribution of atmospheric $CO_2$ accumulation, *Nature*, *398*, 597–601.

Goyet, C., and D. Davis (1997), Estimation of total $CO_2$ concentration throughout the water column, *Deep Sea Res., Part I*, *44*, 859–877.

Gregg, M. C. (1998), Estimation and geography of diapycnal mixing in the stratified ocean, in *Physical Processes in Lakes and Oceans, Coastal Estuarine Stud.*, vol. 54, edited by J. Imberger, pp. 305–338, AGU, Washington, D. C.

Harrison, D. E. (1996), Vertical velocity in the central tropical Pacific—A circulation model perspective for JGOFS, *Deep Sea Res., Part II*, *43*, 687–705.

Johnson, E. S. (1996), A convergent instability wave front in the central tropical Pacific, *Deep Sea Res., Part II*, *43*, 753–778.

Johnson, G. C. (2001), The Pacific Ocean subtropical cell surface limb, *Geophys. Res. Lett.*, *28*, 1771–1774.

Johnson, G. C., and M. J. McPhaden (1999), Interior pycnocline flow from the subtropical to the equatorial Pacific Ocean, *J. Phys. Oceanogr.*, *29*, 3073–3089.

Johnson, G. C., M. J. McPhaden, and E. Firing (2001), Equatorial Pacific Ocean horizontal velocity, divergence, and upwelling, *J. Phys. Oceanogr.*, *31*, 839–849.

Johnson, G. C., B. M. Sloyan, W. S. Kessler, and K. E. McTaggart (2002), Direct measurements of upper ocean currents and water properties across the tropical Pacific Ocean during the 1990's, *Prog. Oceanogr.*, *52*, 31–61.

Kennan, S. C., and P. J. Flament (2000), Observations of a tropical instability vortex, *J. Phys. Oceanogr.*, *30*, 2277–2301.

Lu, P., J. P. McCreary Jr., and B. A. Klinger (1998), Meridional circulation cells and the source waters of the Pacific Equatorial Undercurrent, *J. Phys. Oceanogr.*, *28*, 62–84.

Lukas, R. (1986), The termination of the Equatorial Undercurrent in the eastern Pacific, *Prog. Oceanogr.*, *16*, 63–90.

Morel, A., and S. Maritorena (2001), Bio-optical properties of oceanic waters: A reappraisal, *J. Geophys. Res.*, *106*, 7163–7180.

Philander, S. G. H. (1990), *El Niño, La Niña, and the Southern Oscillation*, 289 pp., Academic Press, San Diego, Calif.

Philander, S. G. H., W. J. Hurlin, and A. D. Seigel (1987), Simulation of the seasonal cycle of the tropical Pacific Ocean, *J. Phys. Oceanogr.*, *17*, 1986–2002.

Polito, P. S., J. P. Ryan, W. T. Liu, and F. P. Chavez (2001), Oceanic and atmospheric anomalies of tropical instability waves, *Geophys. Res. Lett.*, *28*, 2233–2236.

Poulain, P.-M. (1993), Estimates of horizontal divergence and vertical velocity in the equatorial Pacific, *J. Phys. Oceanogr.*, *23*, 601–607.

Price, J. F., R. A. Weller, and R. Pinkel (1986), Diurnal cycling: Observations and models of the upper ocean response to diurnal heating, cooling, and wind mixing, *J. Geophys. Res.*, *91*, 8411–8427.

Price, J. F., R. A. Weller, and R. R. Schudlich (1987), Wind-driven ocean currents and Ekman transport, *Science*, *238*, 1534–1538.

Proehl, J. A. (1998), The role of meridional flow asymmetry in the dynamics of tropical instability, *J. Geophys. Res.*, *103*, 24,579–24,618.

Qiao, L., and R. H. Weisberg (1995), Tropical instability wave kinematics: Observations from the Tropical Instability Wave Experiment, *J. Geophys. Res.*, *100*, 8677–8693.

Quay, P. (1997), Was a carbon balance measured in the equatorial Pacific during JGOFS?, *Deep Sea Res., Part II*, *44*, 1765–1781.

Reverdin, G., C. Frankignoul, E. Kestenare, and M. J. McPhaden (1994), Seasonal variability in the surface currents of the equatorial Pacific, *J. Geophys. Res.*, *99*, 20,323–20,344.

Sabine, C., R. A. Freely, G. C. Johnson, and P. G. Strutton (2004), A mixed layer carbon budget for the GasEx-2001 experiment, *J. Geophys. Res.*, *109*, C08S05, doi:10.1029/2002JC001747, in press.

Schudlich, R. R., and J. F. Price (1992), Diurnal cycles of current, temperature, and turbulent dissipation in a model of the equatorial upper ocean, *J. Geophys. Res.*, *97*, 5409–5422.

Smith, T. M., and R. W. Reynolds (1998), A high-resolution global sea surface temperature climatology for the 1961–90 base period, *J. Clim.*, *11*, 3320–3323.

Strutton, P. G., J. P. Ryan, and F. P. Chavez (2001), Enhanced chlorophyll associated with tropical instability waves in the equatorial Pacific, *Geophys. Res. Lett.*, *28*, 2005–2008.

Strutton, P. G., F. P. Chavez, R. C. Dugdale, and V. Hogue (2004), Primary productivity in the central equatorial Pacific (3°S 130°W) during GasEx-2001, *J. Geophys. Res.*, *109*, C08S06, doi:10.1029/2003JC001790, in press.

Swenson, M. S., and D. V. Hansen (1999), Tropical Pacific ocean mixed layer heat budget: The Pacific cold tongue, *J. Phys. Oceanogr.*, *29*, 69–81.

Tsuchiya, M. (1968), Upper waters of the intertropical Pacific Ocean, *Johns Hopkins Oceanogr. Stud.*, *4*, 1–50.

Weisberg, R. H., and L. Qiao (2000), Equatorial upwelling in the central Pacific estimated from moored velocity profilers, *J. Phys. Oceanogr.*, *30*, 105–124.

Wyrtki, K. (1981), An estimate of equatorial upwelling in the Pacific, *J. Phys. Oceanogr.*, *11*, 1205–1214.

Wyrtki, K., and B. Kilonsky (1984), Mean water and current structure during the Hawaii-to-Tahiti shuttle experiment, *J. Phys. Oceanogr.*, *14*, 242–254.

Yu, X., and M. J. McPhaden (1999), Seasonal variability in the equatorial Pacific, *J. Phys. Oceanogr.*, *29*, 925–947.

————————————

J. M. Hummon, Department of Oceanography, University of Hawaii, 1000 Pope Road, Honolulu, HI 96822, USA.

G. C. Johnson, K. E. McTaggart, and C. L. Sabine, NOAA Pacific Marine Environmental Laboratory, 7600 Sand Point Way NE, Building 3, Seattle, WA 98115-6349, USA. (gregory.c.johnson@noaa.gov)